

# Persistence Curves: A canonical framework for summarizing persistence diagrams

Yu-Min Chung and Austin Lawson  
Department of Mathematics and Statistics  
University of North Carolina at Greensboro

June 3, 2022

## Abstract

*Persistence diagrams* are a main tool in the field of Topological Data Analysis (TDA). They contain fruitful information about the shape of data. The use of machine learning algorithms on the space of persistence diagrams proves to be challenging as the space is complicated. For that reason, summarizing and vectorizing these diagrams is an important topic currently researched in TDA. In this work, we provide a general framework of summarizing diagrams that we call *Persistence Curves* (PC). The main idea is so-called Fundamental Lemma of Persistent Homology, which is derived from the classic *elder rule*. Under this framework, certain well-known summaries, such as persistent Betti numbers, and persistence landscape, are special cases of the PC. Moreover, we prove a rigorous bound for a general families of PCs. In particular, certain family of PCs admit the stability property under an additional assumption. Finally, we apply PCs to textures classification on four well-know texture datasets. The result outperforms several existing TDA methods.

## 1 Introduction

Topological data analysis (TDA) is a relatively new field of mathematics that seeks to examine the shape and structure of data. Persistent homology (PH) is an important tool in TDA developed in 2002 [18] based on the work of size functions in the 1990's [21, 20]. Since its inception, TDA has permeated through many disciplines. Indeed applications of TDA can be found in neuroscience [3], medical biology [28], sensor networks [14], social networks [8], physics [16], computation [30], nanotechnology [33], and more.

Persistent homology transforms a data set into a sequence of topological spaces, called a filtration, where it tracks when features, such as holes and components, appear (are born) and disappear (die). Collecting this birth-death information leads to a visual summary called a persistence diagram. Intuitively, the amount of time a hole or component exists, called the lifespan, indicates

the relative importance of the associated feature. For many applications, this intuition holds though it is not always necessarily the case [3]. By using the bottleneck distance, one can consider the metric space of persistence diagrams. We cannot easily use machine learning methods or other common data analysis methods on this metric space as it has a multi-set structure and was shown to have very little other structure [32]. However, there exist methods to transform persistence diagrams into something more palatable for these analytics methods.

## 2 Recent Work

Summarizations of persistence diagrams can be placed into two main categories: kernel estimation and vectorization. In the former, one constructs a kernel function, or a rule for measuring and quantifying the likeness of two persistence diagrams. This method has been seen through a bag-of-words [27] and kernel SVM for persistence [38]. To vectorize a persistence diagram is to map it into a certain Hilbert space. This summarization type has been well-studied in the forms of Persistence Landscapes [5], Persistence Images [1], Persistent Entropy [2], Euler Characteristic Curve [39], etc. Persistence Landscapes provides a stable (which we will define in Section 4.3) functional representation of a diagram, which maps a diagram to an element in  $L^2$ . PL has many applications. Persistence Images [1] provides a stable way to transform persistence diagrams through the placement of small surfaces over each diagram point. Persistent Entropy defines an entropy derived from the information theory, and provides a stable summary of persistence diagrams. Euler Characteristics Curve, and Betti number curve have been studied and used before the theory of persistent homology was developed. These two summarization methods are not mutually exclusive and have been combined via Persistence Codebooks [41]. We present a vectorization method, and apply it to texture analysis.

Texture analysis is a fundamental task in many scientific areas, such as image processing, material science [6], geology [37], brain disease [23], thyroid nodules [25], and more. There have been studies on texture classifications by TDA tools [27, 22, 9, 38]. Our approach is different from those, and is simpler to implement. Most importantly, in many cases our approach outperforms those results.

In creating a summary method for persistence diagrams, one wishes for the summary to have a few important qualities. Adams, et. al [1] neatly outline the qualities of a good vectorization method as follows:

**Problem Statement.** “How can we represent a persistence diagram so that

1. The output of the representation is a vector in  $\mathbb{R}^n$ ;
2. The representation is stable with respect to the input noise;
3. The representation is efficient to compute;
4. The representation maintains an interpretable connection to the original persistence diagram;

5. The representation allows one to adjust the relative importance of points in different regions of the persistence diagram.”

The framework we propose in this paper, persistence curves, possesses the above five properties.

### 3 Contribution

In Sections 4 we provide necessary background from the field of TDA, namely cubical homology and persistent homology. In Section 5 we present such a vectorization called persistence curves. The general definition of persistence curves allows them to readily output real vectors of any size hence making them very compatible with machine learning techniques. By making natural choices, we will see persistence curves carry interpretable information about the diagram and hence the underlying space from which the diagram arises. We also show that the representation allows one to adjust relative importance based on regions of a diagram. Finally, we prove a general stability theorem and a useful Corollary. In Section 6, we provide experimental evidence of the computational efficiency of these curves and compare the performance of various persistence curves with other TDA methods on four popular texture databases: Outex [19], UIUCTex[35], KTH Texture under varying illumination, pose, and scale (KTH-TIPS) 2[31], and the Flickr Material Database (FMD)[40]. With Section 7, we end the paper by presenting many possible avenues for the advancement of persistence curves.

## 4 Background

In order to keep this article as self-contained as possible, we introduce and discuss necessary notions and notations of algebraic topology in this section. We begin with cubical complexes and homology, and persistent homology. Much of this section follows the discussion in [15]. For a more detailed introduction, see, for example, [24] for cubical homology and [17] for persistent homology.

### 4.1 Binary, Gray-scale, and Color Images

Our main applications in this paper involve texture analysis via gray-scale and color images. Cubical complex is one of the most intuitive way to represent and study images. For that reason, we review the theory of cubical complex and homology in this section. There are several ways to represent the shape of an object, such as simplicial complexes [17]. Complexes are ways to represent the space of the underlying objects. From complexes, persistent homology can be built. Persistence curves are applications of persistence diagrams. It should be noted that cubical homology is just one of many homology theories. The method of persistent homology does not depend on the type of homology theory chosen. Hence, the method of persistence curves will not depend on this choice either.

Formally, an  $n \times m$  **grayscale image** is a function

$$I : \{0, 1, \dots, n-1\} \times \{0, 1, \dots, m-1\} \rightarrow \{0, 1, \dots, 255\}.$$

We associate grayscale images as a collection of tiny squares called pixels each with a shade of gray called the pixel values. In this case, the pixel in the  $i$ -th row and the  $j$ -th column has a pixel value of  $I(i, j)$ . One may view a binary image as an image whose codomain is the set  $\{0, 1\}$ . In this case we associate 0 with the color black and 1 with the color white. Equivalently, one could also view binary images as sets. Points in the set will be white, while those are not in the set will be black. In this paper, we consider binary images in this way. For a grayscale image  $I(i, j)$ , we construct the **binary image** as the sublevel set of  $I$

$$I_t(i, j) = \{(i, j) \mid I(i, j) \leq t\}, \text{ for } t = 0, 1, \dots, 255.$$

## 4.2 Cubical Homology

Homology provides a discrete object as a descriptor of a topological space. As a topological invariant, the homology of a topological space is stable under continuous deformations. This means that the homology of a space gives us useful information about its structure. Though homology is not as strong as invariants like homotopy or homeomorphisms, the complexity (or lack thereof) of its computability makes it a feasible tool for applications. Recall that binary images are the collection of squares from which we obtain a topological summary by counting clusters of white pixels (connected components) and clusters of black pixels (holes). These numbers are called *Betti numbers*. Although the formal definition of Betti numbers will be given at the end of this section, their intuition can be described in a concrete example as shown in Figure 1. In particular, in this work, we are interested in shapes built up by white pixels inside binary images. In Figure 1(a), we have a binary image that has 4 white regions, and hence, the 0-th level Betti number is 4, i.e.  $\beta_0 = 4$ . Moreover, there are two black regions that were enclosed by the white regions, and hence, the first level Betti number is 2, i.e.  $\beta_1 = 2$ . In some cases, one may want to consider the shapes built up by black pixels. In this case, one may take the complement of the binary image (interchanging the colors) as shown in Figure 1(b). Notice however doing so does not simply flip  $\beta_0$  and  $\beta_1$ . This means the complement image, gives additional information and we will see that information is worth considering. To understand Betti numbers formally, we consider intervals of the form  $[\ell, \ell+1]$  or  $[\ell, \ell] := [\ell] = \{\ell\}$  where  $\ell \in \mathbb{Z}$ , these are called **elementary intervals**. Intervals of the form  $[\ell]$  are called **degenerate**. We define an **elementary cube** to be a finite product of such intervals. In other words,  $Q$  is an elementary cube if  $Q = J_1 \times J_2 \times \dots \times J_n$  where  $J_j$  is an elementary interval for  $j = 1, \dots, n$ . We let  $\mathcal{K}$  represent the collection of all elementary cubes. We say the set  $X$  is **cubical** if it can be written as a finite union of elementary cubes. For example, one may consider pixels as elementary cubes. More precisely, let  $(i, j)$  be a pixel of a 2D binary image. We view  $(i, j)$





(a) The Betti numbers of a binary image. By convention a binary image represents the cubical complex  $X$  of white pixels in the image, and its Betti number is  $\beta_0(X) = 4$  and  $\beta_1(X) = 2$ . Note that if the image is surrounded a boundary of white pixels, then  $\beta_0(X) = 5$  and  $\beta_1(X) = 3$ .



(b) The image represents the cubical complex  $X$  that arises from the complement of the image in (a). Its Betti numbers are  $\beta_0(X) = 3$  and  $\beta_1(X) = 4$  whether or not there is an assumed boundary of white pixels.

Figure 1: An illustration of Betti numbers and the boundary effect.

as an elementary cube  $[i, i + 1] \times [j, j + 1]$ . Binary images are unions of cubes of  $[i, i + 1] \times [j, j + 1]$  types, and hence, binary images are cubical. By way of notation we define the set  $\mathcal{K}(X) = \{Q \in \mathcal{K} \mid Q \subset X\}$ . Now that we have a basic topological framework, we seek to provide a complementary algebraic framework. For this, we fix a ring  $R$  and cubical set  $X$ . We define the  $k$ -th **chain module** over  $X$ , denoted  $C_k(X)$  to be the formal span of its elementary cubes of dimension  $k$ . In other words, by defining  $\mathcal{K}_k(X) = \{Q \in \mathcal{K}(X) \mid \dim Q = k\}$ , where  $\dim Q$  is the number of non-degenerate intervals in  $Q$ , we see

$$C_k(X; R) = \left\{ \sum_{Q \in \mathcal{K}_k(X)} \alpha_Q Q \mid \alpha_Q \in R \right\}.$$

Note that since  $\mathcal{K}_k(X)$  is finite, this defines an  $R$ -module for each  $k \in \mathbb{N}$ . Each element of a chain module is called a **chain**. The **support** of a chain is simply the elementary cubes with nonzero coefficients. Naturally then, we would like some way to connect these chain modules over all dimensions. To do this, we need the **algebraic boundary map**,  $\partial$ . We define this map in pieces. For any interval  $[\ell, \ell + 1]$ ,  $\partial([\ell, \ell + 1]) := [\ell + 1] - [\ell]$  and  $\partial([\ell]) = 0$  for every degenerate interval. Now that we understand the map for intervals, we define  $\partial$  for elementary cubes:

$$\partial(J_1 \times J_2 \times \dots \times J_m) = \sum_{j=1}^m J_1 \times \dots \times \partial(J_j) \times \dots \times J_m,$$

where if  $J_j = [\ell, \ell + 1]$  we have

$$J_1 \times \dots \times \partial(J_j) \times \dots \times J_m = J_1 \times \dots \times [\ell + 1] \times \dots \times J_m - J_1 \times \dots \times [\ell] \times \dots \times J_m,$$

and in the case  $J_j$  is degenerate, we obtain 0. A fundamental proposition of boundary maps is the following.

**Proposition 1.** [24] *For any elementary cube  $Q$ , one has  $\partial\partial Q = 0$ .*

In fact, this operator extends naturally to a linear operator on the chain modules. In particular, given a chain  $c = \sum_{i=1}^m \alpha_i Q_i$  [24] we see

$$\partial(c) = \sum_{i=1}^m \alpha_i \partial(Q_i).$$

Thus we see  $\partial\partial c = 0$ . Notice also a single application of  $\partial$  reduces the embedding dimension by at least 1. This means now  $\partial|_{C_k(X;R)} := \partial_k : C_k(X;R) \rightarrow C_{k-1}(X;R)$  is a map from the  $k$ -chain module to the  $(k-1)$ -chain module. Thus given a cubical set  $X$  we can construct the **chain complex**  $\mathcal{C}(X;R) = \{(C_k(X;R), \partial_k) \mid k \in \mathbb{N}\} \cup \{0\}$  which is the collection of all  $k$ -chain modules along with their boundary maps along with the zero space. To avoid notation overload, we will write  $C_k$  for  $C_k(X;R)$  when the context is clear. We can realize a chain complex as the following sequence

$$\dots \xrightarrow{\partial_3} C_2 \xrightarrow{\partial_2} C_1 \xrightarrow{\partial_1} C_0 \xrightarrow{\partial_0} 0.$$

Now we call the kernel,  $\ker \partial_k$ , of the  $k$ -th boundary map to be the  **$k$ -cycles** or just **cycles** and the image  $\text{im } \partial_k$  to be the  $k+1$ -boundary or just **boundary**. Notice that because  $\partial\partial \equiv 0$  we have  $\text{im } \partial_k$  is a normal additive subgroup of  $\ker \partial_{k+1}$ . Hence we define the  $k$ -th homology group of  $\mathcal{K}$  to be

$$H_k(X;R) = \ker \partial_k / \text{im } \partial_{k+1}.$$

This gives rise to the mantra: “homology equals cycles mod the boundaries.” We call the rank (or order) of the  $k$ -th homology group the  **$k$ -th Betti number** and write  $\beta_k(X;R)$ . Intuitively, the  $k$ -th Betti number tells us how many  $k$ -dimensional holes our underlying space has. The 0-th level Betti number counts the number of connected components, the first level Betti number counts the number of “circles” we have and the second level Betti number counts the number of “air pockets” or “spheres” the space has and so on.

### 4.3 Persistent Homology

At this point, we see the formal definition of Betti number and how to count them for a given set. The main application in this paper is to analyze texture images. However, we cannot directly compute or define the homology of a grayscale or color image, since grayscale or color images are functions rather than sets. This naturally leads to the development of the persistent homology. To study the shapes of functions, one common way is to consider sublevel sets (4.1) [20, 21]. There is a parameter  $t$  that one may have to make the choice of. In general, selecting a parameter (such as  $t$  in (4.1)) can be a difficult

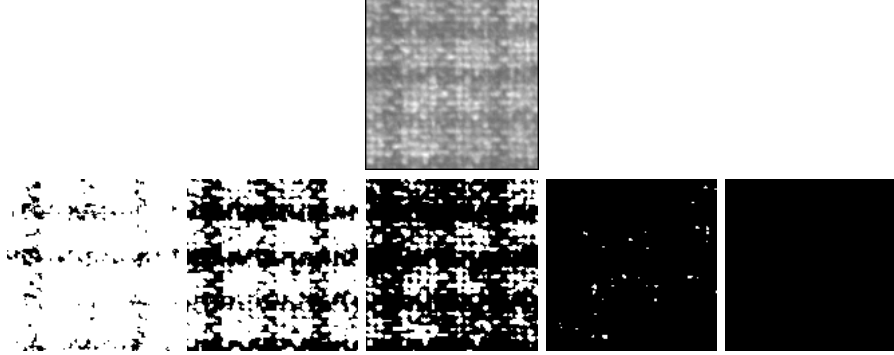


Figure 2: A grayscale image from Outex and a filtration representing the image

task. Persistent homology removes the need for choice and considers many parameter values at once, thereby creating a robust theory. We need to be careful about the way we consider many threshold values. Suppose  $X$  represents a cubical set and let  $\mathcal{K}$  represent the corresponding cubical complex. We define a function  $f : \mathbb{R} \rightarrow \mathcal{K}$  and require that whenever  $a \leq b$ , we have  $f(a) \subset f(b)$ . Such a function is called a **filtering function**. Let  $(a_1, a_2, \dots, a_n)$  be a finite increasing sequence of real numbers where  $f(a_n) = \mathcal{K}$ . Then a **filtration** of  $\mathcal{K}$  is the corresponding sequence  $f(a_1) \subset f(a_2) \subset \dots \subset f(a_n)$ . An image  $I$  has a natural filtration associated to it by considering the sequence  $I_1 \subset I_2 \subset \dots$ . We create a filtering function for  $I$  by the function  $f(t) \mapsto \mathcal{K}(\text{im } I_t)$ .

Suppose that we have a filtration of a cubical complex,

$$\mathcal{K}_1 \subset \mathcal{K}_2 \subset \dots \subset \mathcal{K}_n.$$

The inclusion induces homomorphism between the homology groups so that for each  $k$  we have

$$H_k(\mathcal{K}_1) \xrightarrow{i_1^*} H_k(\mathcal{K}_2) \xrightarrow{i_2^*} \dots \xrightarrow{i_{n-1}^*} H_k(\mathcal{K}_n),$$

where each  $i_k^*$  is a homomorphism. We say a homology class  $\alpha$  is **born** at  $j$  if we have  $\alpha \in H_k(\mathcal{K}_j)$  and  $\alpha \notin i_{j-1}^*(H_k(\mathcal{K}_{j-1}))$ . We say  $\alpha$  dies at  $H_k(\mathcal{K}_j)$  if  $\alpha \in H_k(\mathcal{K}_{j-1})$  and one of the following hold:

- $i_{j-1}^*(\alpha)$  is trivial; or
- if  $\alpha$  is born at  $j$  and  $\beta$  is born at  $\ell < j$  and  $f_{i^*-1}(\alpha) = f_{i^*-1}(\beta)$ .

In the last condition we employ the **elder rule**, which allows us to uniquely define the death of a class. This rule says in the choice between two classes, we choose to keep the “oldest” class. We can guarantee that every homology class  $\alpha \in H_k(\mathcal{K}_j)$  for some  $j$  has a birth time. We cannot guarantee that each class has a death time. For such classes, we assign the “death time” as  $\infty$ . This procedure

allows us to define a unique set of points for each homology class  $(b, d)$  where  $b$  is the birth time of the class and  $d$  is its death time. We will define the persistence diagram, but first let us recall the concept of a multi-set. A **multi-set** is a set  $S$  along with a **multiplicity function**  $M : S \rightarrow \mathbb{N} \cup \{\infty\}$ , we denote a multi-set by the tuple  $(S, M)$ . Suppose we have a filtering function  $f$  of a cubical set  $X$ . A **persistence diagram** is a multi-set  $\mathcal{P}_k(X, f) = (P_k, M_k)$  where  $P_k$  consists of all unique birth-death pairs along with the diagonal  $\{(x, x) \mid x \in \mathbb{R}\}$  and  $M_k$  assigns the multiplicity of the birth-death pairs and  $M_k(x, x) = \infty$  for each diagonal element. An example of a diagram can be found in Figure 3(c)-(d). We will often denote  $\mathcal{P}_k(X, f)$  by  $\mathcal{P}_k$  when the context is obvious. Figure 3 shows an example of persistence diagrams of a grayscale image. Although Figure 3(a) is a grayscale image, visual inspection suggests that there are 8 “white” pieces and 4 “black” holes. Its persistence diagrams as shown in Figure 3(c)-(d) confirms the intuition. There are 8 (4) points that are away from the diagonal line in  $\mathcal{P}_0$  ( $\mathcal{P}_1$ ), and that suggests they persist for a long period of thresholds. Hence, they are likely the robust features.

We would like to know that this summary of our data is stable in some sense. For us, this means that if we perturb the original points by a small amount, we want the diagrams to different by a small amount. This so-called stability theorem is the cornerstone of persistent homology. A natural question arises: how can one measure the difference of persistence diagrams?

To answer this question we turn our attention to the **Wasserstein p-metric**  $W_p$  for  $1 \leq p \leq \infty$ , which we define as follows. Given two diagrams  $D_1 = \mathcal{P}_k(X, f)$  and  $D_2 = \mathcal{P}_k(Y, g)$

$$W_p(D_1, D_2) = \inf_{\substack{\text{bijections} \\ \eta: D_1 \rightarrow D_2}} \left( \sum_{x \in D_1} \|x - \eta(x)\|^p \right)^{1/p},$$

for  $1 \leq p < \infty$  and

$$W_\infty(D_1, D_2) = \inf_{\substack{\text{bijections} \\ \eta: D_1 \rightarrow D_2}} \sup_{x \in D_1} \|x - \eta(x)\|.$$

The Wasserstein  $\infty$ -metric is also known as **bottleneck distance**. The Wasserstein distance searches over all possible pairings to find an optimal one. It should be noted that an optimal pairing is not necessarily unique. Given the necessity of the bijections  $\eta$ , it now becomes apparent, why we need the diagonal to have infinite multiplicity. Otherwise, a pairing would not be possible. This brings us to the popular stability theorem that states that the bottleneck distance is 1-Lipschitz with respect to the  $\infty$ -norm on the filtering functions. That is to say if  $X$  is a cubical set then

$$W_\infty(\mathcal{P}_k(X, f), \mathcal{P}_k(X, g)) \leq \|f - g\|_\infty.$$

The proof of which first appeared in [12]. We end this section with a note that cubical homology and sublevel sets are just one example of many processes

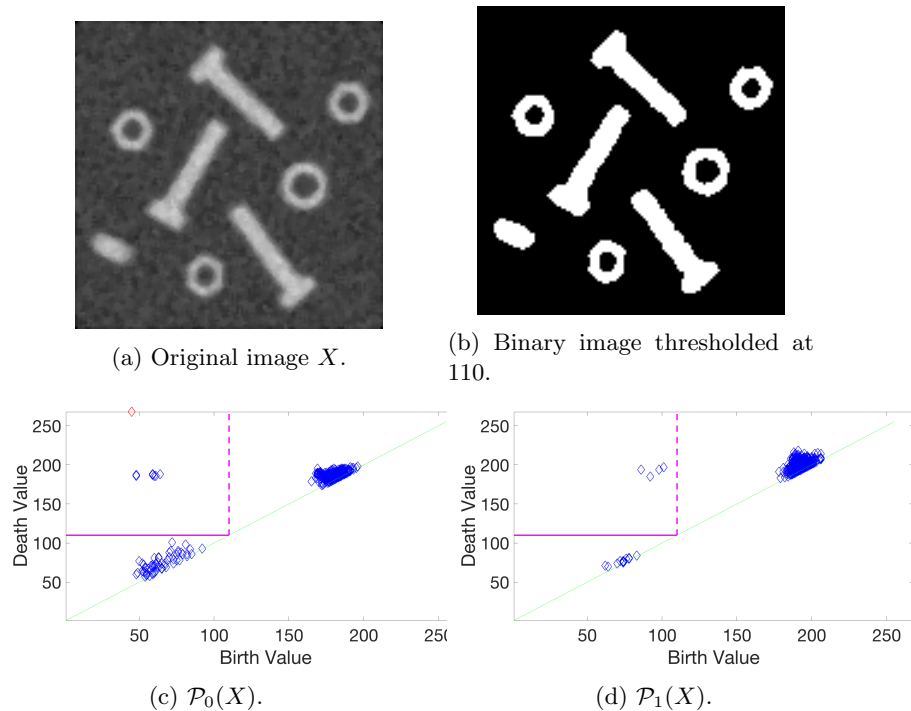


Figure 3: A toy example of persistence diagrams of a grayscale image. (a) By visual inspection, one expects the Betti numbers are  $(8, 4)$ . (b) Binary image is obtained from thresholding the  $X$  at 110. Betti number of this binary image are  $(8, 4)$ . (c)-(d) Persistence diagrams of  $X$ . The rectangular boxes enclosed by the pink dotted and solid line are the fundamental boxes defined in (1).  $\beta_0(X_{110}) = 8$  and  $\beta_1(X_{110}) = 4$ .

by which persistence diagrams arise. In the following section, we will present persistence curves, which rely on persistence diagrams and not the process by which they were created.

## 5 Persistence Curves and Stability

This section contains the main idea to construct the persistence curves. The essential idea is the Fundamental Lemma of Persistent Homology [17] which is derived from the elder rule. This lemma states that given a filtering function  $f$  on a space  $X$ , one has the following calculation for the corresponding  $k$ -dimensional diagram  $D_k$ ,

$$\beta_k(f(t)) := \beta(t) := \#\{(b, d) \in D_k \mid b \leq t, d > t\}, \quad (1)$$

where  $\#$  represents the counting measure. Figure 3(c)-(d) shows an example of (1). In particular, the rectangular boxes in (c)-(d) enclosed by the dotted line

represents the set  $\{(b, d) \in D_k \mid b \leq 110, d > 110\}$  for  $k = 0, 1$ , respectively. It is straightforward to observe that  $\#\{(b, d) \in D_0 \mid b \leq 110, d > 110\} = 8$  and  $\#\{(b, d) \in D_1 \mid b \leq 110, d > 110\} = 4$ , which are the Betti numbers of Figure 3(b) by visual inspection. However, (1) does not fully utilize the information of the set. Thus we seek to generalize (1) in the following way. Let  $\mathcal{D}$  represent the set of all persistence diagrams. let  $\mathcal{F}$  represent the set of all functions  $\psi : \mathcal{D} \times \mathbb{R}^3 \rightarrow \mathbb{R}$  so that  $\psi(D; x, x, t) = 0$  for all  $x \in \mathbb{R}$ . Let  $\mathcal{T}$  represent the set of **statistics** or operators on multi-sets; more precisely, any  $T \in \mathcal{T}$  is a map that takes a multi-set into a scalar. Finally let  $\mathcal{R}$  represent the set of functions on  $\mathbb{R}$ .

**Definition 1.** We define a map  $P : \mathcal{D} \times \mathcal{F} \times \mathcal{T} \rightarrow \mathcal{R}$  where

$$P(D, \psi, T)(t) = T(\{\psi(D; b, d, t) \mid b \leq t, d > t\}), t \in \mathbb{R}.$$

The function  $P(D, \psi, T)$  is called a **persistence curve** on  $D$  with respect to  $\psi$  and  $T$ .

To better understand persistence curves, we begin by discussing examples.

**Example 1.** Let  $\mathbf{1}(x, y, t) = 1$  if  $x \neq y$  and 0 otherwise. Let  $T$  be the summation operator,  $\Sigma$ . By Definition 1, we have

$$\begin{aligned} P(D, \mathbf{1}, \Sigma) &= \sum(\{\mathbf{1}(D; b, d, t) \mid b \leq t, d > t\}) \\ &= \#\{(b, d) \in D \mid b \leq t, d > t\} = \beta(t). \end{aligned}$$

Furthermore, if  $D_0, D_1, \dots, D_k, \dots$  are the  $k$ -dimensional diagrams associated to a given filtration  $\mathcal{X}$ . Using the Fundamental Lemma of Persistent Homology, we may define the **Euler Characteristic** of the space  $X_t$  corresponding to a threshold  $t$  is the alternating sum of the space's Betti numbers. That is,

$$EC(X_t) := EC(t) = \sum_{i=0}^{\infty} (-1)^i \beta_i(t) = \sum_{i=0}^{\infty} (-1)^i P(D_i, \mathbf{1}, \Sigma)(t).$$

The term **Euler Characteristic Curve** with respect to the filtration  $\mathcal{X}$  refers to the function

$$ECC(X) \equiv \sum_{i=0}^{\infty} (-1)^i P(D_i, \mathbf{1}, \Sigma).$$

Next, we will discuss a non-trivial example.

**Example 2.** Let  $\psi = d - b$  and  $T$  be the  $\Sigma$ , the summation operator. Then the  $P(D, \psi, \Sigma) = \sum(\{d - b \mid b \leq t, d > t\})$ . Figure 4 illustrates  $P(D, \psi, \Sigma)$ . Figure 4 shows the a life curve and at 5 selected threshold values, we see the set  $\{d - b \mid b \leq t, d > t\}$ . The value of the curve at that threshold if calculated by applying  $\psi$  to each highlighted point and summing over all such function values. In the content of grayscale images, this curve can be interpreted as the lifespan at the current binary image.

Here are some examples that are independently studied in different contents, but they can be realized as persistence curves.

**Example 3.** [10] developed an optimal thresholding method in imaging processing based on persistence diagrams. The main idea in [10] is to define an objective function, and the optimal threshold will be chosen at the maximum of the objective function. One major component of the objective function in [10] is  $\Phi(t) = \frac{1}{\#D(t)} \sum_{(b,d) \in D(t)} (d-t)(t-b)$ , where  $D(t) = \{d-b \mid b \leq t, d > t\}$ .  $\Phi(t)$  can be viewed as persistence curves if one lets  $\psi = (d-t)(t-b)$  and  $T$  be the average operator, then  $P(D, \psi, T) = \Phi(t)$ .

Another example is by [2], where the concept of entropy was introduced to TDA.

**Example 4.** In [2], a summary function based on persistence entropy was defined  $S(D)(t) = -\sum w(t) \frac{d-b}{L} \log(\frac{d-b}{L})$ , where  $L = \sum (d-b)$  and  $w(t) = 1$  if  $b \leq t \leq d$  and  $w(t) = 0$  otherwise. Let  $\psi = -\frac{d-b}{\sum (d-b)} \log \frac{d-b}{\sum (d-b)}$ , and  $T = \Sigma$ . Then we find that  $E(D) := P(D, \psi, T)$  is similar to  $S(D)$ . In fact due to the exclusion of the death value in the interval we have  $0 \leq E(D) \leq S(D)$ . Hence  $E(D)$  enjoys the same stability as proven in [2].

In this last example, we also recognize persistence landscapes, a well-known diagram summary, as a special case of persistence curves.

**Example 5.** Let  $\max_k(S)$  represent the  $k$ -th largest number of a set  $S$ . [5] defines the following functions for a diagram  $D$ .

$$f_{(b,d)}(t) = \begin{cases} 0 & \text{if } t \notin (b, d) \\ t-b & \text{if } t \in (b, \frac{b+d}{2}] \\ d-t & \text{if } t \in (\frac{b+d}{2}, d) \end{cases}$$

Then the  $k$ -th Persistence Landscape [5] is defined by  $\lambda_k(t) = \max_k \{f_{(b,d)}(t) \mid (b,d) \in D\}$ . We see then with  $\psi(b,d,t) = \min\{t-b, d-t\}$  and  $T = \max_k$ ,  $P(D, \psi, T) \equiv \lambda_k$ . Indeed one can quickly see through direct calculation that  $\psi \cdot w(b,d,t) \equiv f_{(b,d)}(t)$ .

We see that under the Persistence Curve framework, two seemingly disparate object, namely the Betti curve and persistence landscapes, are connected.

Although we have the ability to choose any function of the diagrams, we tend to choose the functions that carry sensible information about the diagram and hence the underlying space. Many of these curves are built from well-studied persistence diagram statistics. Table 1 lists a few persistence curves that rely on well-studied diagram statistics. For example, the **Midlife** quantity has been used in recent work, such as persistence landscapes [5] and persistence image [1] to serve as a linear transformation. The **Multiplicative Life** quantity has been studied in the field of random complexes [4]. The life-entropy persistence curve actually appears as the entropy summary function in a recent paper by

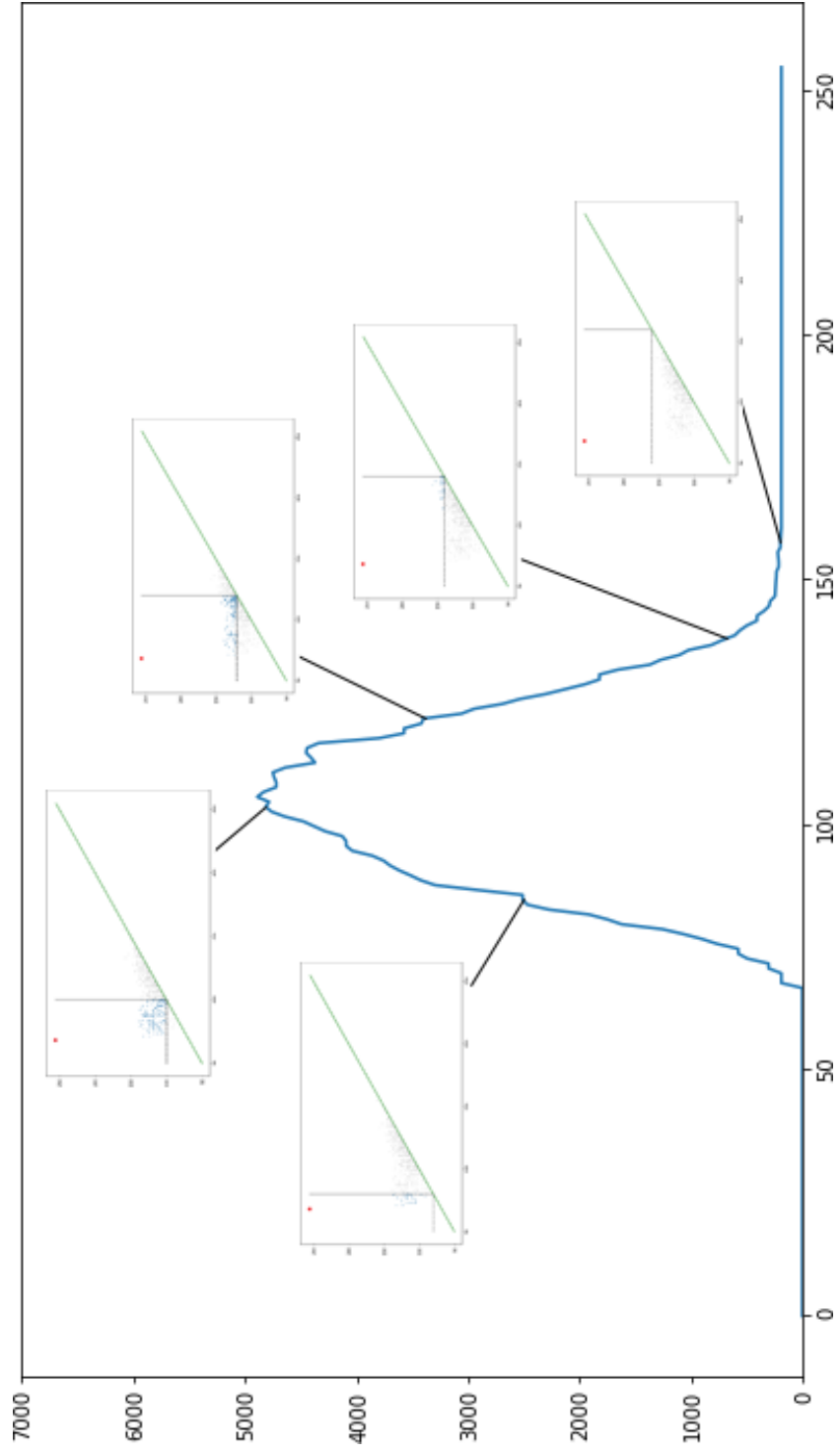


Figure 4: Schematic of a persistence curve,  $P(D, d - b, \Sigma)$ . Each subplot represents the set  $\{(b, d) \mid b \leq t, d > t\}$ .



Name	Notation	$\psi(b, d, t)$	T
Betti	$\beta(D)$	1	sum
Midlife	$\mathbf{ml}(D)$	$(b + d)/2$	sum
Life	$\ell(D)$	$d - b$	sum
Multiplicative Life	$\mathbf{mul}(D)$	$d/b$	sum
Life Entropy [2]	$\mathbf{le}(D)$	$-\frac{d-b}{\sum(d-b)} \log \frac{d-b}{\sum(d-b)}$	sum
Midlife Entropy	$\mathbf{mle}(D)$	$-\frac{d+b}{\sum(d+b)} \log \frac{d+b}{\sum(d+b)}$	sum
Mult. Life Entropy	$\mathbf{mule}(D)$	$-\frac{d/b}{\sum(d/b)} \log \frac{d/b}{\sum(d/b)}$	sum
$k$ -th Landscape [5]	$\lambda_k(D)$	$\min\{t - b, d - t\}$	$\max_k$

Table 1: Examples of persistence curves.

Atienza, Gonzales-Diaz, and Soriano-Trigueros [2]. We also introduce two new entropy-like functions using the multiplicative life and midlife statistics.

Notation	Description
$n$	The maximum between the number of off diagonal points in each diagram
$(b_i^D, d_i^D)$	a point in persistence diagram $D$
$\psi_i^D$	$\psi(b_i^D, d_i^D)$
$\Psi^D$	$\sum \psi_i^D$
$w_i^D(x)$	$w(b_i^D, d_i^D, x) = 1$ if $b_i^D \leq x \leq d_i^D$ ; 0 otherwise.
$L^D$	$\sum d_i^D - b_i^D$

Table 2: The notation here pertains to two given diagrams  $C$  and  $D$  enumerated in correspondence to the optimal matching for bottleneck distance

Before our next theorem, we will set up some notation and conventions. Let  $C, D \in \mathcal{D}$ . Let  $n$  represent the maximum between the number of off diagonal points in each diagram and note that  $n$  is finite. We assume the optimal matching under the bottleneck distance of these diagrams is known and we index the points of each diagram  $\{(b_i, d_i)_D\}_{i=1}^n$  and  $\{(b_i, d_i)_C\}_{i=1}^n$  so that

points with matching indices are paired under the optimal matching. We define  $L^D = \sum_{i=1}^n (d_i - b_i)$  and analogously for  $C$ . If  $\psi \in \mathcal{F}$ , we define  $\psi_i^D = \psi(b_i, d_i)$  for  $i = 1, \dots, n$ ,  $\Psi^D = \sum_{i=1}^n \psi(b_i, d_i)_D$ , and  $w_i \equiv w(b_i, d_i, \cdot)$  again, analogously for  $C$ . Notice that if  $T$  is the sum statistic, then  $P(D, \psi, T)(t)$  can be written as

$$\sum_{(b,d) \in D} \psi(b, d, t) w(b, d, t) = \sum_{i=1}^n \psi_i^D w_i^D$$

For easy reference, this notation is summed up in Table 2. Finally, in regards to infinite death values one has a couple options. If there is a global maximum finite death value for the space, we set all infinite death values to this maximum. For example, in the case of images, 255 is the max pixel value, hence the largest possible finite death value. If no such value exists, we can set the infinite death values to be equal to the largest finite death value in the current filtration.

**Theorem 1.** *Let  $C, D \in \mathcal{D}$  and index them through the optimal bottleneck distance matching. Let  $T$  be the sum statistic. We adopt the notations in Table 2. Let  $\psi \in \mathcal{F}$  and*

$$\epsilon := \min\{L^C \max_i |\psi_i^C - \psi_i^D| + 2\Psi^D W_\infty(C, D), L^D \max_i |\psi_i^C - \psi_i^D| + 2\Psi^C W_\infty(C, D)\}.$$

Then we have

$$\|P(C, \psi, T) - P(D, \psi, T)\|_1 \leq \epsilon.$$

*Proof.* We are interested in the difference.

$$\|P(C, \psi, T) - P(D, \psi, T)\|_1 = \left\| \sum_{i=1}^n \psi_i^D w_i^D - \sum_{i=1}^n \psi_i^C w_i^C \right\|_1$$

This becomes

$$\begin{aligned} \|P(D, \psi, T) - P(C, \psi, T)\|_1 &= \left\| \sum_{i=1}^n \psi_i^D w_i^D - \sum_{i=1}^n \psi_i^C w_i^C \right\|_1 = \left\| \sum_{i=1}^n \psi_i^D w_i^D - \psi_i^C w_i^C \right\|_1 \\ &\leq \sum_{i=1}^n \|\psi_i^D w_i^D - \psi_i^C w_i^C\|_1 \leq \sum_{i=1}^n \|w_i^C\|_1 |\psi_i^C - \psi_i^D| + |\psi_i^D| \|w_i^C - w_i^D\|_1. \end{aligned}$$

We'll focus on each summand individually. Notice that  $w_i$  is simply the indicator function on the interval  $[b_i, d_i)$ , hence its norm is just the lifespan of the corresponding diagram point,  $d_i - b_i$ . Thus we see for the first,

$$\sum_{i=1}^n \|w_i^C\|_1 |\psi_i^C - \psi_i^D| \leq \sum_{i=1}^n \|w_i^C\|_1 \max_i |\psi_i^C - \psi_i^D| \leq L^C \max_i |\psi_i^C - \psi_i^D|.$$

The dichotomous nature of  $w_i$  allows us to write  $w_i^D = w_i^D w_i^C + w_i^D (1 - w_i^C)$  and vice versa for  $w_i^C$ . For the second summand we note that  $\|w_i^C - w_i^D\|_1 \leq \|w_i^D (1 - w_i^C)\|_1 + \|w_i^C (1 - w_i^D)\|_1$  and  $w_i^D (1 - w_i^C) = 1 \Rightarrow w_i^C (1 - w_i^D) = 0$ . In consideration of the pairing  $(b_i^C, d_i^C), (b_i^D, d_i^D)$  there are three cases to consider up to permutation. Those cases are

- 1)  $b_i^C \leq d_i^C \leq b_i^D \leq d_i^D$ ;
- 2)  $b_i^C \leq b_i^D \leq d_i^C \leq d_i^D$ ;
- 3)  $b_i^C \leq b_i^D \leq d_i^D \leq d_i^C$ .

In each case, it is straightforward to observe that

$$\|w_i^D(1-w_i^C)\|_1 + \|w_i^C(1-w_i^D)\|_1 \leq 2 \cdot \max_i \{|b_i^C - b_i^D|, |d_i^C - d_i^D|\} \leq 2 \cdot W_\infty(C, D).$$

Thus, we have

$$\sum_{i=1}^n |\psi_i^D| \|w_i^C - w_i^D\|_1 \leq \sum_{i=1}^n |\psi_i^D| (2 \cdot \max_i \{|b_i^C - b_i^D|, |d_i^C - d_i^D|\}) \leq 2\Psi^D W_\infty(C, D).$$

Hence, we obtain

$$\|P(D, \psi, T) - P(C, \psi, T)\|_1 \leq L^C \max_i |\psi_i^C - \psi_i^D| + 2\Psi^D W_\infty(C, D).$$

However, we must note that there was a choice of splitting in the beginning. Therefore, with

$$\epsilon = \min\{L^C \max_i |\psi_i^C - \psi_i^D| + 2\Psi^D d_\infty(C, D), L^D \max_i |\psi_i^C - \psi_i^D| + 2\Psi^C W_\infty(C, D)\},$$

we conclude

$$\|P(D, \psi, T) - P(C, \psi, T)\|_1 \leq \epsilon.$$

□

Note that there is no assumption on  $\psi$ . Theorem 1 offers a general bound on persistence curves associated with different persistence diagrams. It does not reveal the stability (yet). As we will discuss in Section 6, unstable persistence curves may also serve reveal important and useful topological information, such as ECC. On the other hand, if the stability is of the interest, with an additional assumption on  $\psi$ , the stable persistence curves can be obtained as stated below.

**Corollary 1.** *Under the same assumptions as in Theorem 1, if we further assume that  $\psi$  is a stable measurement, i.e.  $\|\psi^C - \psi^D\| \leq KW_\infty(C, D)$ , then the persistence curves are stable, i.e.*

$$\|P(C, \psi) - P(D, \psi)\| \leq \tilde{K} W_\infty(C, D). \quad (2)$$

where  $\tilde{K} = \min\{KL^C + 2\Psi^D, KL^D + 2\Psi^C\}$

*Proof.* It follows directly from Theorem 1. □

For example, if  $\psi = \mathbf{1e}$ , the stability result due to [2] can be retrieved from Corollary 1.

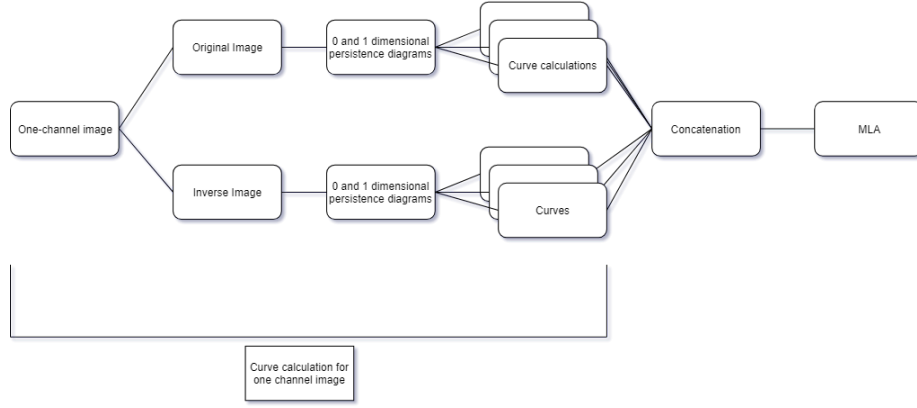


Figure 5: PC workflow for one channel image

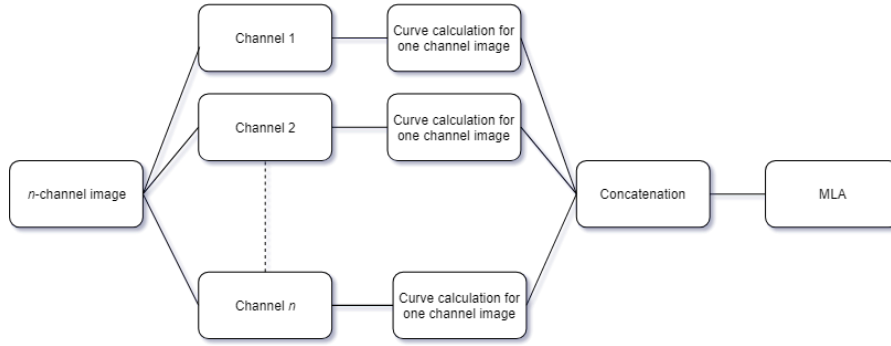


Figure 6: PC workflow for  $n$ -channel image

**Theorem 2.** [2] Let  $C, D$  be diagrams. Let  $L_{min} = \min\{L^C, L^D\}$ ,  $L_{max} = \max\{L^C, L^D\}$ ,  $N = \max\{n^C, n^D\}$  and  $r_\infty(C, D) = \frac{2NW_\infty(C, D)}{L_{max}}$  (this is called the relative error of  $C$  and  $D$ ), then

$$\|P(C, \mathbf{le}) - P(D, \mathbf{le})\|_1 \leq 2r_\infty(C, D) \left( \log[2r_\infty(C, D)] + L_{max} \frac{\log N}{N} \right).$$

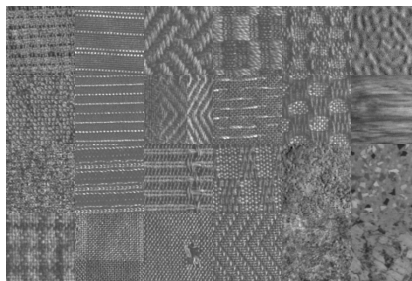
Thusfar we have established the concept of a persistence curve, established a general bound, and established a class of persistence curves based on stable measurements that are robust with respect to noise.

## 6 Applications to texture analysis

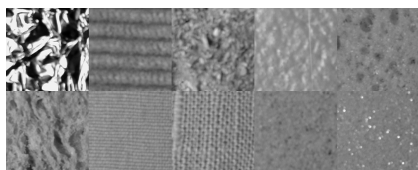
In this section, we apply PCs to texture classification. Texture analysis is one of the fundamental research areas in computer vision. (yu-min: talk about texture



(a) A snapshot of the 25 different textures in UIUCTex.



(b) A snapshot of the 24 textures in Outex.

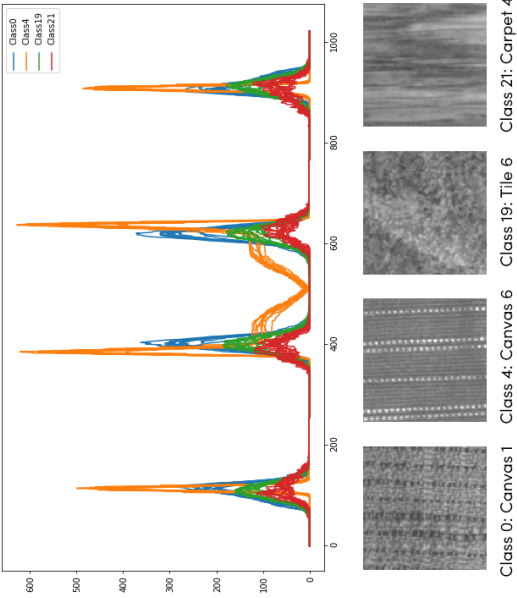


(c) A snapshot of the 10 textures of KTH-TIPS.

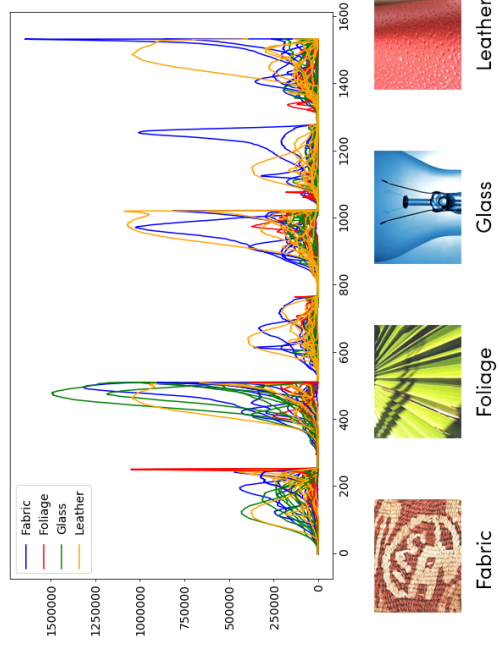


(d) A snapshot of the 10 textures in the FMD database.

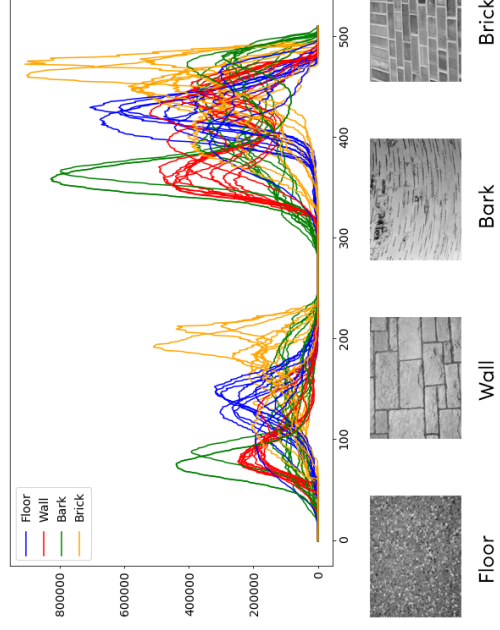
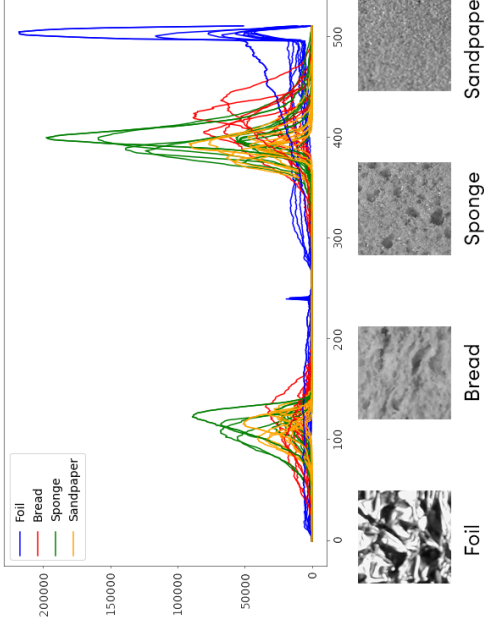
Figure 7: Snapshots of the texture databases



(a) A sample of 4 textures from Outex Test suite 0 and their corresponding Betti curves calculated on 0 and 1 dimensional diagrams for each image and its inverse.



(c) A sample of 4 textures from FMD and their corresponding Betti curves.



(d) A sample of 4 textures from UIUCTex and their corresponding Betti curves.

analysis here) One challenge in the area is to find intrinsic characteristics, or quantitative representations of textures in order to perform classifications, or employ statistics. PCs can be served as intrinsic characteristics of the textures, and this section is devoted to demonstrating effectiveness of PCs.

## 6.1 Descriptions of the data

We consider 4 popular texture databases and describe each of them below.

- (i) **Outex** is a database from the University of Oulu and consists of 15 test suites each with a different challenge [19]. We focus on the test suites 0, 3, and 10. Test suite 0 contains 24 texture classes with 20 images of each class that are 128 by 128 in size. The test suite 0 is equipped with 100 preset 50-50 train/test splits. A score on the test suite 0 is the average accuracy over all 100 splits. Test suite 3 is similar to 0 with the only difference in the misclassification costs. A score on the test suite 3 is the average weighted accuracy over the 100 splits. Finally, Test suite 10 tests rotational invariance (yu-min: Say more about it). In this suite there is a single train/test split of the 4320 images with the training set containing 1/9 of the images. A score on this test suite is a single accuracy score. See Figure 7(b) for sample images of Outex.
- (ii) **UIUC** dataset is a collection of textures from University of Illinois Urbana-Champaign [26]. The dataset consists of 25 texture classes with 40 images of each texture. Each image is of size 640 by 480. A score on this set is the average accuracy of 100 random 50-50 train/test splits. See Figure 7(a) for sample textures from UIUCTex.
- (iii) **KTH-TIPS 2** [31] The KTH Textures under varying Illumination, Pose and Scale (TIPS) 2 is a database containing 81 200 by 200 grayscale images for each of its 10 textures. As the name suggests, each texture class contains images of different scales, rotations, and illuminations. A score on this set is the average accuracy of 100 random 50-50 train/test splits. See Figure 7(c) for sample textures from KTH-TIPS 2.
- (iv) **FMD** The Flickr Material Database (FMD) contains 100 RGB images of sizes 512 by 384 for each of its 10 materials [40]. This database is the most challenging as it focuses more on material recognition, i.e. the classes contain images of many different objects at different scales. A score on this set is the average accuracy of 100 random 50-50 train/test splits. See Figure 7(d) for sample textures from KTH-TIPS 2.

Outex, UIUCTex, KTH-TIPS consist of gray-scale images; FMD consists of color images in the standard RGB channel.

## 6.2 Classification

In order to illustrate the effectiveness of PCs, we keep our classification pipeline and model simple. Overall speaking, for each image, we calculate persistence

diagrams, compute persistence curves, and feed PCs as features into machine learning algorithms (MLA), as shown in Figure 5. We use two MLAs in this article—support vector machine (SVM) and random forest (RF). Since the intensity values of images range from 0 to 255, each PC is a vector in  $\mathbb{R}^{256}$  associated with the standard Euclidean distance. For each image, there are two persistence diagrams,  $D_0$  and  $D_1$ . We find it useful to consider the image and its complement. More precisely, consider the image  $I^C(i, j) := 255 - I(i, j)$ . Topologically, taking both  $I$  and  $I^C$  into account is similar to consider both sub-level and super-level sets of  $I$ . As shown in Figure 1, this example shows that  $I^C$  may carry more information than single  $I$  may do.

Table 3: Performance on FMD

Curves/MLA	SVM	RF
$(\beta, \beta\mathbf{S})$	31.8	38.6
$(\text{le}(I), \text{le}(I^C))$	34.5	41.7
$(\text{mul}(I), \text{mul}(I^C))$	34.1	39.2
$(\text{le}(I), \text{le}(I^C), \text{mule}(I), \text{mule}(I^C), \text{mle}(I), \text{mle}(I^C))$	38.8	41.3
$(\text{le}(I), \text{le}(I^C), \text{mle}(I), \text{mle}(I^C))$	37.1	39.7
$(\text{le}(I), \text{le}(I^C), \text{mule}(I), \text{mule}(I^C)) + \text{PS} ([11])$	33.2	44.5
Persistence Landscapes (PL)	30.1	32.9
$(\text{PL}, \text{le}(I), \text{le}(I^C), \text{mule}(I), \text{mule}(I^C))$	25.7	41.8
$(\text{PS}, \text{PL}, \text{le}(I), \text{le}(I^C), \text{mule}(I), \text{mule}(I^C))$	33.6	43.4
$(\text{PS}, \text{PL})$	33.4	42.9

As examples, we illustrate the Betti curves on images and their complements for 4 different textures in the databases in Figures 8a, 8d, 8b, and 8c. From each figure, we observe that Betti curves of the same type of textures are of a similar pattern. For instance, Figure 8a shows a sample of 4 textures from Outex. 0 to 255 is  $\beta_0(I)$  curve; 256 to 511 is  $\beta_1(I)$ ; 512 to 767 is  $\beta_0(I^C)$ ; 768 to 1023. At this point, since we see that PCs can served as characteristics of textures, they will be the main features in our classification model.

Table 4 compares the performance of various persistence curves, the Euler Characteristic Curve, and other TDA methods from the literature on the 4 databases. Up to our best knowledge, those TDA methods were applied to Outex 0; one of them were applied to UIUCTex and KTH.

For our applications we consider PCs described in Table 1, and their combinations. There are five different sets of features in Table 4 which consist of ECC,  $\beta$ , le, mul, mule, and mle. The first two sets (Row 1 and 2 in Table 4 do not require persistent homology. As discussed in [39], Betti numbers and ECC are useful descriptors.

First, we focus on the results of the Outex. We compared our methods with those developed in [22, 38, 27, 7, 9] where they applied their TDA methods to Outex 0. Those performances were directly from their work [36]. From Table 4, we see that ECC and Betti curves perform well on Outex, but not so



well on UIUCTex or KTH. One possible explanation for this is these two curves are less stable than, say, the entropy curves. Hence, with the introduction of variation within a particular class (as in UIUC and KTH), performance is hindered. We also see that the Betti curve outperforms ECC. This makes sense as the Betti curves do not lose information through addition and subtraction as ECC does. We see once we consider the entropy curves, not only do we have high performance, we also have consistency across these data sets. PC falls slightly short of the Outex benchmark. We must note that the Outex benchmarks vary between the test suites. For Outex 0 and 3, the benchmark uses Gabor filtering [?]. With Outex 10, the benchmark model is a Local Binary Pattern with Variance [?]. In this table we also see other TDA Methods. Sparse-TDA and kernel-TDA are both kernel methods. CLBP-SMC is also a kernel method that utilizes the Local Binary Patterns method. The Sliced Wasserstein Kernel,  $k_{PSS}$ , is another kernel method that proves to perform best out of the TDA methods on Outex 0. Another kernel method, EKFC+LMNN is a vectorization method that computes a descriptor based on the topology of a klein bottle, then combines this set of vectors with a metric learned through Large Margin Nearest Neighbors [36]. This method is able to achieve high scores on UIUC and KTH. We see Persistence Curves perform on a level similar to these high performing TDA methods, with the added benefit of their simplicity and generalized framework.

When we evaluate on more complex databases, such as UIUCTex, we see the scores begin to favor the entropy curves. Examining these texture databases reveal more variation of the images within each respective class. These scores suggest that there is a trade-off between the variation within a class and the performance of the more stable curves.

### 6.3 Combination of Persistence statistics

Among these 4 databases, the FMD is the most challenging one. Unlike the other databases we consider, the FMD consists of RGB color images of 10 different materials. Within each class these materials will have different colors and even different textures. Our main task is to find characteristics capable of distinguishing between these materials. To do this, we treat each color channel (R, G, and B) as a single gray scale image. We generate our chosen persistence curves as shown in Table 7 on each of these channels and their complements. Among PC features, the best classification performance by SVM is 38.8% (with entropy curves) as shown in Table 7. The best classification performance by RF uses the same model and achieves a 41.3% recognition rate. This result is comparable to those in [29].

To improve to classification performance, we consider *persistence statistics*(PS) [11]. The concept of PS has been used in several work [ref? RBC and SW]. Persistence statistics summarize diagrams by assigning them to a single number. For example, the average lifespan of the birth-death pairs in a diagram is one such statistic. For each of the 12 diagrams (0 and 1 dimensional for each of the 3 channels and their inverses) we construct the datasets of death

plus birth and lifespan. On each of these sets we calculate the mean, median, standard deviation, skewness, kurtosis, the 10th, 25th, 75th, 90th percentiles. Each of these values are concatenated to our persistence curves. Because we are combining both local and global features for these persistence diagrams, the concern for weighting the importance of these values arises. For this reason we turn to the machine learning algorithm known as random forests (RF). In short, a random forest is an ensemble method that combines a (possibly) large number of decision trees. This method allows us to forgo the weighting of these global values. Table 7 reveals the performance FMD. We used a variety of methods including the use of SVM and also the use of Persistence Landscapes [5]. This model was constructed by averaging the first 6 landscapes evaluated at the values  $0, 1, \dots, 255$ . We see immediately that RF outperforms SVM in each scenario. Moreover, we again see that the combination of the entropy curves perform well and are only improved by the addition of persistence statistics. With the addition of Persistence Statistics, we see a decrease in the SVM recognition rate due to weighting issues. However, we see that RF has an increased recognition rate of 44.5%. We note this score is achieved using raw images and without any weight or parameter/hyper-parameter tuning. Persistence curves not only enjoy simplicity of concept and implementation, but also enjoy high performance potential.

## 6.4 Efficiency and Limitations

The computational efficiency of persistence curves depends on the chosen curve, the number of points in a given diagram, and the number of points at which the curve is evaluated. From the Definition 1, we observe that the complexity of computing PC is roughly linear in both threshold and number of generators. The first experiment is to confirm this observation. For experimentation purposes, we examine the **mule**. We generate random diagrams in the following way. Each birth value is sampled from a uniform distribution on the interval 0 to 100. To each birth value  $b$ , we assign a death value by sampling a uniform distribution on the interval  $b$  to 101. We perform two experiments. First, we fix 1000 equidistant points in the interval 0 to 100. For each  $n$  in  $\{10, 50, 100, 500, 1000, 5000, 10000, 50000, 100000, 500000, 1000000\}$  we generate 100 random diagrams with  $n$  points in the method described above. From here, we measure the average time taken to calculate the **mule** curve on each of these 100 diagrams at the 1000 equidistant points. In the second experiment we fix the number of points in a generated diagram at 1000. Then for each  $m$  in  $\{10, 50, 100, 500, 1000, 5000, 10000, 50000\}$  we generate 100 random diagrams each with 1000 points. We calculate the average time to calculate the **mule** curve at  $m$  equidistant points on the interval 0 to 100. The results of these experiments appear in Tables 5 and 6 as well as Figure 11. We see experimentally, the computation of persistence curves is quite efficient with linear complexity in both experiments.

It is important to note that these persistence curves have some limitations. Because diagrams are not unique to a particular space, different textures may

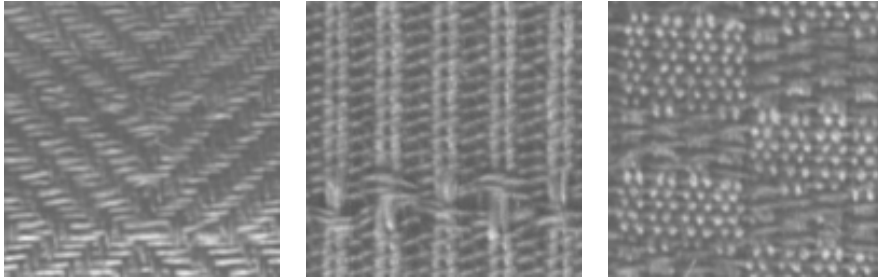
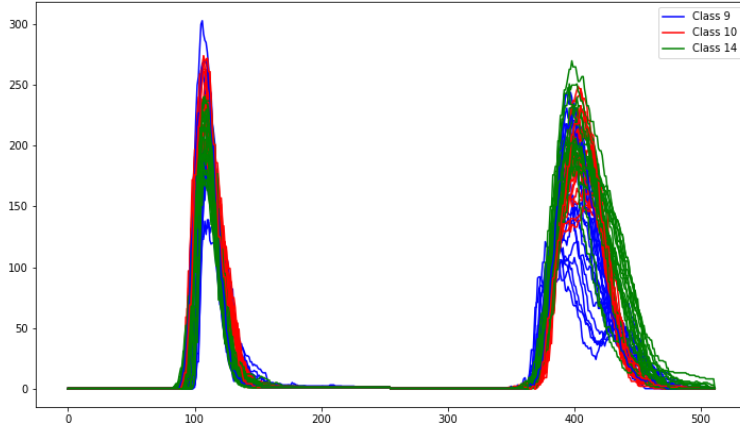


Figure 9: These three images represent the most frequently misclassified classes Outex 0 and the corresponding Betti curves.

have similar persistence diagrams. This inverse problem is a challenging problem, and is a new research area in TDA [13, 34]. To illustrate this, we generate two images as shown in Figure 10. To the human eye, these look like images of two different textures, but they actually produce the exact same persistence diagram. While it is unlikely that real textures will produce exactly the same diagram, it is possible for different textures to produce similar diagrams hence similar persistence curves. For example in Figure 9 we see 3 different classes of canvas texture in Outex 0. These 3 classes most often confused the classifiers. The rotational and size invariance of the topological descriptors play a role in this confusion as we see these textures have similar patterns in different sizes and orientations.

Proposed Features	Outex0	Outex3	Outex10	UIUC	KTH
ECC( $I$ )	96.7	96.6	96.2	70.2	75.5
$[\beta(I), \beta(I^C)]$	97.9	98.0	97.2	80.8	78.3
$[\text{le}(I), \text{le}(I^C)]$	96.6	96.8	96.6	85.4	87.5
$[\text{mul}(I), \text{mul}(I^C)]$	96.2	96.0	96.0	83.6	82.2
$[\text{le}(I), \text{le}(I^C), \text{mle}(I), \text{mle}(I^C)]$	97.7	97.9	97.2	88.8	90.8
Outex Benchmark	99.5	99.5	97.9	-	-
Other TDA methods	Outex 0	Outex 3	Outex 10	UIUC	KTH
sparse-TDA [22]	66.0	-	-	-	-
Kernel-TDA [38]	69.2	-	-	-	-
CLBP-SMC [27]	87.5	-	-	-	-
$k_{PSS}$ [7]	98.8	-	-	-	-
Persistence Paths [9]	97.8	-	-	-	-
EKFC+LMNN [36]	-	-	-	91.23	94.77

Table 4: In the table, we use the curve name to indicate the name of the classifier. An ‘S’ appearing at the end of a curve indicates the curve is calculated on inverses. a number  $k$  in front of a curve indicates the curve is multiplied by  $k$ . The scoring mechanism for Outex is provided by each test suite. UIUCTex and KTH-TIPS2 were both scored by performing 100 50-50 stratified train/test splits then averaging the resulting scores.

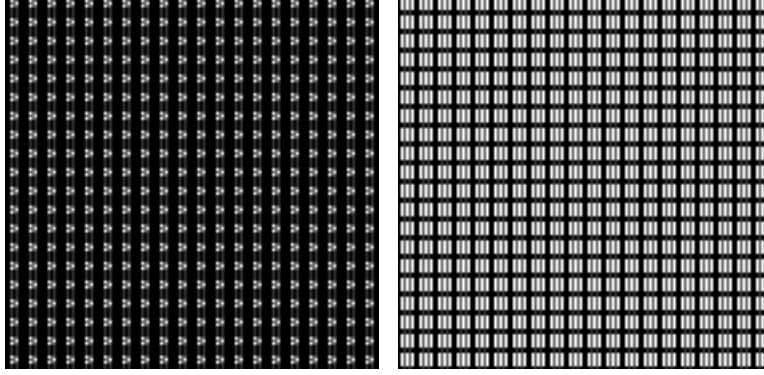


Figure 10: The two figures above have different textures, yet they yield the same persistence diagrams.

Diagram points	1000	5000	10000	50000	100000	500000	1000000
Time (in seconds)	0.007	0.034	0.068	0.376	0.719	3.415	6.735

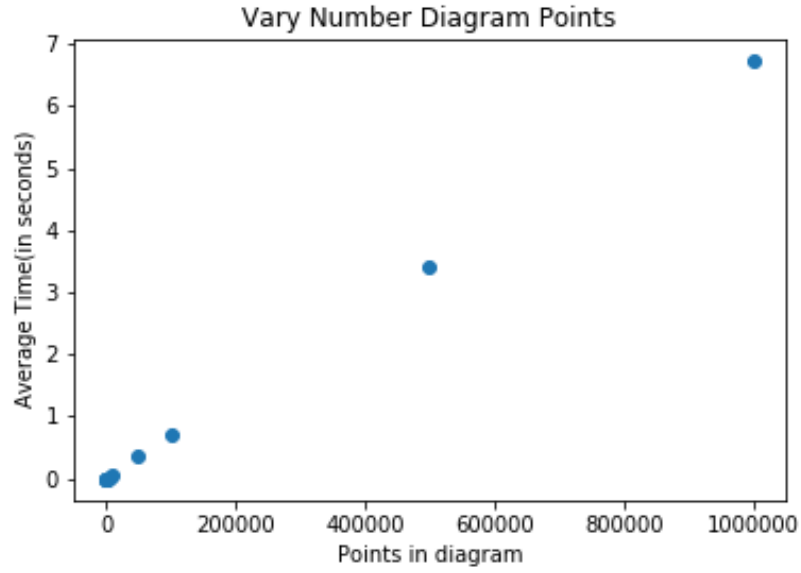
Table 5: Average time over 100 random diagrams with prescribed number of points to compute **mule** curve at 1000 points

Mesh points	100	500	1000	5000	10000	50000
Time (in seconds)	0.026	0.045	0.068	0.240	0.452	2.141

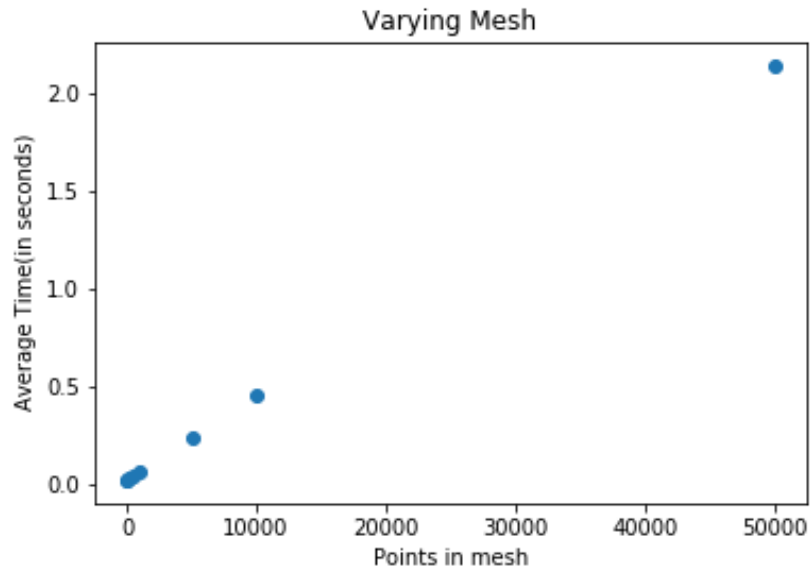
Table 6: Average time over 100 random diagrams with 100 points to compute **mule** curve at prescribed number of points

Curves/MLA	SVM	RF
$(\beta, \beta S)$	31.8	38.6
$(le, leS)$	34.5	41.7
$(mul, mulS)$	34.1	39.2
$(le, leS, mule, muleS, mle, mleS)$	38.8	41.3
$(le, leS, mle, mleS)$	37.1	39.7
$(le, leS, mule, muleS) + \text{Persistent Statistics (PS)} ([11])$	33.2	44.5
Persistence Landscapes (PL)	30.1	32.9
$(PL, le, leS, mule, muleS)$	25.7	41.8
$(PS, PL, le, leS, mule, muleS)$	33.6	43.4
$(PS, PL)$	33.4	42.9

Table 7: Performance on FMD



(a) Average time over 100 random diagrams with prescribed number of points to compute **mule** curve at 1000 points



(b) Average time over 100 random diagrams with 100 points to compute **mule** curve at prescribed number of points

Figure 11: Computation time experiment

Curve	UIUCTex	Noisy UIUCTex
Beta	80.8	80.5
le	85.4	85.2
mul	83.6	83.4
entropies	88.8	88.8

Table 9: Caption

Curve	Outex 0	Noisy Outex 0
$(\beta, \beta\mathbf{S})$	97.9	97.3
$(\mathbf{le}, \mathbf{leS})$	96.6	96.5
$(\mathbf{mul}, \mathbf{mulS})$	96.2	95.6
$(\mathbf{le}, \mathbf{leS}, \mathbf{mule}, \mathbf{muleS}, \mathbf{mle}, \mathbf{mleS})$	97.7	96.4
$(4\beta, 4\beta\mathbf{S}, \mathbf{mlt}, \mathbf{mltS}, \mathbf{lm}, \mathbf{lmS})$	99.0	77.9

Table 8: For Outex 0, we added Gaussian noise to the images. We trained on the true images, then tested on the noisy images. We quickly note that the curves are generally stable. The final curve, which incorporates the Life/Mid curve is clearly unstable.

Noise generation was essentially adding a random matrix with about 38% chance of being 0, 24% of being 1, 24% -1, 6% of being 2, 6% of being -2, and a 1% chance of being 3, 1% chance of being -3 with negligible percentage for integers of higher magnitude. Essentially performing a round to nearest integer on standard normal.

## 7 Generalization and Conclusion

Persistence curves provide a simple general framework from which we can construct usable models for data analysis that retain the topological information contained in the persistence diagrams they are calculated from. In addition, these curves are compatible with machine learning, they are stable, they are efficient to compute, and by choice of function and statistic, one can alter the importance of points in different regions of the persistence diagrams. We have also shown that these curves create useful classifiers for texture analysis. The theory and experimentation presented here are by no means complete. In fact there is a rich future for the study of persistence curves.

**Questions.** We present some open questions in no particular order.

- Q1 Like Persistence Landscapes, what other vectorizations can be viewed as a special case of the Persistence Curves?
- Q2 What conditions on the function  $\psi$  or the statistic  $T$  can lead to a more general and useful stability result?

- Q3 Is there a statistical framework to perform “curve selection” that will produce an optimal or near optimal set of curves for modeling?
- Q4 Could weighting be used to improve performance? In particular, is there a nice way to combine the local Persistence Curves with the global Persistent Statistics?
- Q5 In what other areas might Persistence Curves be useful?

## References

- [1] Henry Adams, Tegan Emerson, Michael Kirby, Rachel Neville, Chris Peterson, Patrick Shipman, Sofya Chepushtanova, Eric Hanson, Francis Motta, and Lori Ziegelmeier. Persistence images: A stable vector representation of persistent homology. *The Journal of Machine Learning Research*, 18(1):218–252, 2017.
- [2] Nieves Atienza, Rocío González-Díaz, and M. Soriano-Trigueros. On the stability of persistent entropy and new summary functions for TDA. *CoRR*, abs/1803.08304, 2018.
- [3] Paul Bendich, James S Marron, Ezra Miller, Alex Pieloch, and Sean Skwerer. Persistent homology analysis of brain artery trees. *The annals of applied statistics*, 10(1):198, 2016.
- [4] Omer Bobrowski, Matthew Kahle, Primož Skraba, et al. Maximally persistent cycles in random geometric complexes. *The Annals of Applied Probability*, 27(4):2032–2060, 2017.
- [5] Peter Bubenik. Statistical topological data analysis using persistence landscapes. *The Journal of Machine Learning Research*, 16(1):77–102, 2015.
- [6] H-J Bunge. *Texture analysis in materials science: mathematical methods*. Elsevier, 2013.
- [7] Mathieu Carrière, Marco Cuturi, and Steve Oudot. Sliced Wasserstein kernel for persistence diagrams. In Doina Precup and Yee Whye Teh, editors, *Proceedings of the 34th International Conference on Machine Learning*, volume 70 of *Proceedings of Machine Learning Research*, pages 664–673, International Convention Centre, Sydney, Australia, 06–11 Aug 2017. PMLR.
- [8] Corrie J Carstens and Kathy J Horadam. Persistent homology of collaboration networks. *Mathematical problems in engineering*, 2013, 2013.
- [9] Ilya Chevyrev, Vidit Nanda, and Harald Oberhauser. Persistence paths and signature features in topological data analysis. *arXiv preprint arXiv:1806.00381*, 2018.



- [10] Yu-Min Chung and Sarah Day. Topological fidelity and image thresholding: A persistent homology approach. *Journal of Mathematical Imaging and Vision*, pages 1–13, 2018.
- [11] Yu-Min Chung, Chuan-Shen Hu, Austin Lawson, and Clifford Smyth. Topological approaches to skin disease image analysis. In *2018 IEEE International Conference on Big Data (Big Data)*, 2018 (in press).
- [12] David Cohen-Steiner, Herbert Edelsbrunner, and John Harer. Stability of persistence diagrams. *Discrete & Computational Geometry*, 37(1):103–120, 2007.
- [13] Justin Curry. The fiber of the persistence map. *arXiv preprint arXiv:1706.06059*, 2017.
- [14] Vin De Silva, Robert Ghrist, et al. Coverage in sensor networks via persistent homology. *Algebraic & Geometric Topology*, 7(1):339–358, 2007.
- [15] Paweł Dłotko and Thomas Wanner. Topological microstructure analysis using persistence landscapes. *Physica D: Nonlinear Phenomena*, 334:60–81, 2016.
- [16] Irene Donato, Matteo Gori, Marco Pettini, Giovanni Petri, Sarah De Nigris, Roberto Franzosi, and Francesco Vaccarino. Persistent homology analysis of phase transitions. *Physical Review E*, 93(5):052138, 2016.
- [17] H. Edelsbrunner and J. Harer. *Computational Topology: An Introduction*. Miscellaneous Books. American Mathematical Society, 2010.
- [18] Herbert Edelsbrunner, David Letscher, and Afra Zomorodian. Topological persistence and simplification. In *Proceedings 41st Annual Symposium on Foundations of Computer Science*, pages 454–463. IEEE, 2000.
- [19] Ojala T. et. al. Outex - new framework for empirical evaluation of texture analysis algorithms.
- [20] Massimo Ferri, Patrizio Frosini, Alberto Lovato, and Chiara Zambelli. Point selection: A new comparison scheme for size functions (with an application to monogram recognition). In *Asian Conference on Computer Vision*, pages 329–337. Springer, 1998.
- [21] Patrizio Frosini. Measuring shapes by size functions. In *Intelligent Robots and Computer Vision X: Algorithms and Techniques*, volume 1607, pages 122–134. International Society for Optics and Photonics, 1992.
- [22] Wei Guo, Krithika Manohar, Steven L Brunton, and Ashis G Banerjee. Sparse-tda: Sparse realization of topological data analysis for multi-way classification. *IEEE Transactions on Knowledge and Data Engineering*, 30(7):1403–1408, 2018.

- [23] Maria Del C Valdés Hernández, Victor González-Castro, Francesca M. Chappell, Eleni Sakka, Stephen Makin, Paul A. Armitage, William H. Nailon, and Joanna M. Wardlaw. Application of texture analysis to study small vessel disease and bloodbrain barrier integrity. In *Front. Neurol.*, 2017.
- [24] T. Kaczynski, K. Mischaikow, and M. Mrozek. *Computational Homology*. Applied Mathematical Sciences. Springer New York, 2004.
- [25] Soo-Yeon Kim, Eun-Kyung Kim, Hee Jung Moon, Jung Hyun Yoon, and Jin Young Kwak. Application of texture analysis in the differential diagnosis of benign and malignant thyroid nodules: Comparison with gray-scale ultrasound and elastography. *AJR. American journal of roentgenology*, 205 3:W343–51, 2015.
- [26] Svetlana Lazebnik, Cordelia Schmid, and Jean Ponce. A sparse texture representation using local affine regions. *IEEE Transactions on Pattern Analysis and Machine Intelligence*, 27(8):1265–1278, 2005.
- [27] Chunyuan Li, Maks Ovsjanikov, and Frederic Chazal. Persistence-based structural recognition. In *Proceedings of the IEEE Conference on Computer Vision and Pattern Recognition*, pages 1995–2002, 2014.
- [28] Li Li, Wei-Yi Cheng, Benjamin S Glicksberg, Omri Gottesman, Ronald Tamler, Rong Chen, Erwin P Bottinger, and Joel T Dudley. Identification of type 2 diabetes subgroups through topological analysis of patient similarity. *Science translational medicine*, 7(311):311ra174–311ra174, 2015.
- [29] Ce Liu, Lavanya Sharan, Edward H Adelson, and Ruth Rosenholtz. Exploring features in a bayesian framework for material recognition. In *2010 IEEE Computer Society Conference on Computer Vision and Pattern Recognition*, pages 239–246. IEEE, 2010.
- [30] Seth Lloyd, Silvano Garnerone, and Paolo Zanardi. Quantum algorithms for topological and geometric analysis of data. *Nature communications*, 7:10138, 2016.
- [31] P. Mallikarjuna, Alireza Tavakoli Targhi, Eric Hayman Mario Fritz, Barbara Caputo, and Jan-Olof Eklundh. The kth-tips2 database. Available from: <http://www.nada.kth.se/cvap/databases/kth-tips>.
- [32] Yuriy Mileyko, Sayan Mukherjee, and John Harer. Probability measures on the space of persistence diagrams. *Inverse Problems*, 27(12):124007, 2011.
- [33] Takenobu Nakamura, Yasuaki Hiraoka, Akihiko Hirata, Emerson G Escobar, and Yasumasa Nishiura. Persistent homology and many-body atomic structure for medium-range order in the glass. *Nanotechnology*, 26(30):304001, 2015.

- [34] Steve Oudot and Elchanan Solomon. Inverse problems in topological persistence. *arXiv preprint arXiv:1810.10813*, 2018.
- [35] Michelangelo Paci, Loris Nanni, and Stefano Severi. An ensemble of classifiers based on different texture descriptors for texture classification. *Journal of King Saud University - Science*, 12 2012.
- [36] Jose A Perea and Gunnar Carlsson. A klein-bottle-based dictionary for texture representation. *International Journal of Computer Vision*, 107(1):75–97, 2014.
- [37] Valerie Randle and Olaf Engler. *Introduction to texture analysis: macrotexture, microtexture and orientation mapping*. CRC press, 2014.
- [38] Jan Reininghaus, Stefan Huber, Ulrich Bauer, and Roland Kwitt. A stable multi-scale kernel for topological machine learning. In *Proceedings of the IEEE conference on computer vision and pattern recognition*, pages 4741–4748, 2015.
- [39] Eitan Richardson and Michael Werman. Efficient classification using the Euler characteristic. *Pattern Recognition Letters*, 49:99–106, 2014.
- [40] L. Sharan, R. Rosenholtz, and E. H. Adelson. Material perception: What can you see in a brief glance? *Journal of Vision*, 14, no. 9, article 12, 2014.
- [41] Bartosz Zielinski, Mateusz Juda, and Matthias Zeppelzauer. Persistence codebooks for topological data analysis. *arXiv preprint arXiv:1802.04852*, 2018.